

GT2015-43975

EVALUATION OF RANS AND ZDES METHODS FOR THE PREDICTION OF THREE-DIMENSIONAL SEPARATION IN AXIAL FLOW COMPRESSORS

Ashley D. Scillitoe^{1*}, Paul G. Tucker¹, Paolo Adami²

¹CFD Laboratory, Department of Engineering, University of Cambridge, Cambridge, CB2 1PZ, UK

²Core CFD Team Leader, CFD Methods, Rolls-Royce Deutschland, Eschenweg 11, 15827 Blankenfelde-Mahlow, Germany

ABSTRACT

Regions of three-dimensional separations are an inherent flow feature of the corner formed by the suction surface and end-wall of axial compressors. RANS turbulence models, common in industrial CFD codes, often struggle in these regions. This paper investigates the use of two hybrid RANS/LES methods as alternatives to pure RANS methods.

SA and SST based Zonal DES (ZDES) are applied to a linear blade cascade case, studied experimentally by Gbadebo [1]. The time-averaged results are compared to steady SA, SST and RSM RANS results. SA model corrections for streamline curvature, anisotropy and non-equilibrium effects are also examined. For the ZDES computations the solver is modified to reduce dissipation at low Mach numbers.

Significant uncertainty is observed in the RANS results, with the origin of the suction surface corner separation occurring too far upstream, and the extent of the corner separation significantly over-predicted. The laminar separation bubble and the turbulent reattachment are also missed. Consequently the surface pressure distribution, exit flow angle and total pressure loss predictions are poor. Conversely, the ZDES results were encouraging; with much better predictions of the pressure distribution, exit flow angle and trailing edge boundary layer displacement thickness. Some RANS corrections proved effective, such as the SA model with Rotation/Curvature correction (SA-RC), however all had deficiencies in some areas.

Although the ZDES results are encouraging it is noted that these computations were two orders of magnitude more computa-

tionally expensive due to the high mesh densities and small time-steps required. For the ZDES results quality indexes are examined in order to determine whether the computational mesh used is sufficient in different flow regions. Mesh generation strategies based on using a pre-cursor RANS solution to obtain a modelled energy spectrum and various turbulent length scales to guide mesh refinement are considered. These can provide a quick estimate of the potential computational cost of LES or hybrid RANS/LES computations from a RANS solution.

NOMENCLATURE

| | |
|------------|---|
| α_2 | Exit flow angle |
| β_1 | Inlet blade angle |
| i | Incidence angle |
| p | Pressure |
| ρ | Density |
| Re_c | Chord based Reynolds number |
| c | Blade chord length |
| h | Blade height/span |
| s | Blade pitch |
| t | Time, or blade thickness |
| ϕ | A primitive variable, or blade camber angle |
| γ | Blade stagger angle |
| V_1 | Inflow bulk velocity |
| U_n | Face normal velocity component |
| n | Normal vector |
| E | Total energy per unit volume |
| F, G | Flux vectors |

*Address all correspondence to this author (as2341@cam.ac.uk).

| | |
|---------------|--|
| L^{lp} | Pseudo-Laplacian |
| A_{ij} | Flux Jacobian |
| δ | Boundary layer thickness |
| δ^* | Boundary layer displacement thickness |
| θ | Momentum thickness |
| H | Shape factor |
| C_p | Static pressure coefficient, $(p - p_1) / (\frac{1}{2} \rho U_1^2)$ |
| Y_p | Total pressure loss coefficient, $(p_{01} - p_0) / (\frac{1}{2} \rho U_1^2)$ |
| ε | Smoothing constant |
| d | Wall distance |
| Δ | Grid spacing or filter width |
| k | Turbulent kinetic energy |
| ω | Specific turbulent dissipation |
| L_t | Turbulent length-scale |
| \tilde{s} | Sub-grid activity parameter |
| ν | Kinematic viscosity |
| ν_t | Turbulent viscosity |
| γ_p | Production intermittency |
| γ_d | Destruction intermittency |

Subscripts

| | |
|---|---------------------|
| 0 | Stagnation quantity |
| 1 | Inflow quantity |
| 2 | Exit quantity |

Superscripts

- + Non-dimensional distance, e.g. $y^+ = y\sqrt{\tau_w/\rho}/\nu$

INTRODUCTION

Regions of three-dimensional separations are an inherent flow feature of the corner formed by the suction surface and end-wall of axial compressors. These corner separations cause passage blockage and effectively limit the loading and static pressure rise achievable by the compressor. The flow in these regions can be highly unsteady and vortical, with anisotropic and non-equilibrium turbulence effects common. Thus Reynolds Averaged Navier-Stokes (RANS) turbulence models, often used in industrial CFD codes, can struggle here [2–6]. Unsteady RANS (URANS) may be able to account for some unsteady effects, but the spectral gap between the resolved and modelled scales assumed by such methods is often not present in turbo-machinery [7].

By resolving the complex large scales of turbulence Large Eddy Simulation (LES) offers potentially improved accuracy for such flows. With recent increases in computing power, the application of LES to practical engineering problems is becoming more realistic. However, it is still too computationally expensive for computing industrial scale compressors at realistic Reynolds numbers. There is therefore a need to reduce cost, and hybrid

RANS/LES methods offer a promising alternative here. By using Reynolds Averaged Navier-Stokes (RANS) modelling to account for the near-wall turbulent streaks, the high mesh densities required near walls can be significantly reduced, resulting in substantial cost savings at high Reynolds numbers.

The hybrid RANS/LES approach is becoming increasingly popular, and has recently been applied to a number of turbo-machinery compressor flows [8–10]. However, there are still some questions to be answered, for example Lardeau et al. [11] found that wall-resolved LES computations could not reliably predict the boundary layer transition process until the computational mesh approached a Direct Numerical Simulation (DNS) level of resolution. Therefore it is of interest to examine the implications of this for a hybrid RANS/LES method, and whether it is necessary to use a RANS transition model.

Another question to ask is whether the relatively high cost of using hybrid RANS/LES computations in the design process is justified, or whether applying corrections to RANS models to sensitise them to effects such as streamline curvature is acceptable. There are some that argue that the more elaborate Reynolds Stress Transport (RSM) RANS models may offer a tenable alternative to eddy resolving techniques such as LES for the prediction of complex turbo-machinery flows, for example see Morshbach et al. [12]. However, others such as Lien et al. [13] argue that strong evidence of superior accuracy from RSM's for complex industrial flows isn't yet available. Therefore this is also an area to consider.

Finally, as Tucker and DeBonis [14] note, for LES type methods to be integrated into the design process there is a pressing need for best practice guidelines for hybridisation and meshing to be developed. Various practitioners have proposed methods for designing LES meshes from precursor RANS solutions, and this paper attempts to investigate the application of these to an endwall flow. There is also a need to determine whether a mesh is suitable for an LES type computation, since grid sensitivity studies, based on strong mesh refinement, are impractical for LES. Methods for assessing the quality of an LES mesh are described in the literature, however most have only been used on rather simple canonical flows. This paper investigates the use of such methods on an endwall flow which is more representative of a flow seen in the turbo-machinery industry.

COMPUTATIONAL SET-UP

The computational geometries, meshes and numerical methods used in this investigation are briefly introduced in this section.

Computational Domain

The geometry to be computed is a linear CDA (Controlled Diffusion Aerofoil) cascade investigated experimentally

by Gbadebo [1, 15]. Some geometrical parameters for the cascade are presented in Tab. 1. The cascade blades are typical of high-pressure stator blades found in a modern gas-turbine compressor.

TABLE 1: GEOMETRICAL PARAMETERS FOR THE COMPRESSOR CASCADE.

| Parameter | Value |
|---|--------|
| Chord, c (m) | 0.1515 |
| h/c | 1.32 |
| s/c | 0.926 |
| t/c | 0.1 |
| Camber, φ ($^{\circ}$) | 42.0 |
| Stagger, γ ($^{\circ}$) | 14.7 |
| Inlet blade angle, β_1 ($^{\circ}$) | 41.0 |

The computational domain used to represent the cascade is shown in Fig. 1. The experiment consists of a blade with end-walls. The mean flow was found to be symmetric about the mid-span, therefore for the RANS cases it is sufficient to only compute the grey region shown in Fig. 1. In this case the mid-span is treated as an inviscid wall. To represent the pitch-wise periodicity node-to-node matching periodic boundaries are used. The blade and endwall are set as standard no-slip viscous walls. To avoid spurious waves, a considerable buffer zone is placed downstream of the blade. This increases the number of grid points by about 5%, however avoids the need for specialized non-reflecting boundary conditions.

For the hybrid RANS/LES cases the instantaneous flow field is not expected to be symmetric about the mid-span, therefore it isn't suitable to use an inviscid wall at the mid-span. Instead the domain above the mid-span, shown in blue in Fig. 1, is also computed. The second endwall is treated as an inviscid wall, and the grid is aggressively coarsened in this new domain so that it acts as a buffer zone, preventing spurious reflections back into the domain of interest. This approach only adds 12% to the number of grid points.

An H-O-H mesh topology is used here. For the ZDES mesh 569 points are wrapped around the blade, and 135 points are distributed across the blade span with clustering near the endwall. This leads to a final mesh size of 5.54 million grid points. The following near-wall grid spacings are used; $y^+ \leq 1$, $\Delta x^+ < 130$, and $\Delta z^+ < 215$. These spacings are within the recommended ranges for a Hybrid RANS/LES computation [16].

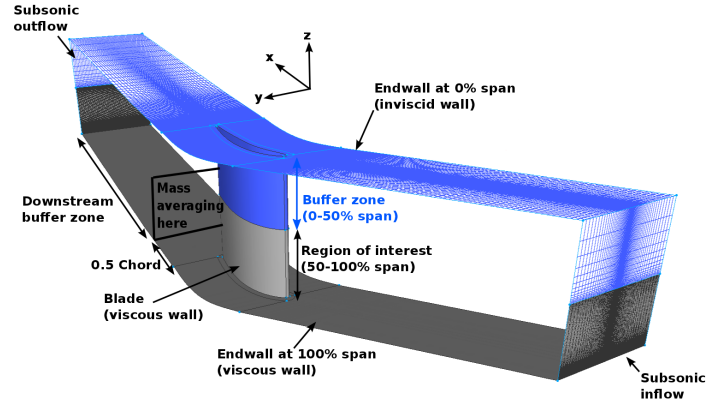


FIGURE 1: COMPUTATIONAL DOMAIN FOR ZDES CASES.

The same grid spacings are used for the RANS mesh, leading to a mesh size of 4.97 million grid points. This is considerably finer than should be required for the RANS computations, in fact Danhua et al. [2] found that only about 630000 grid points were required to achieve a grid independent solution for this case.

Inlet and outlet conditions

To match the inlet measurement position used in the Gbadebo experiment [1] the inlet is located $2c$ upstream of the blade leading edge. The inlet flow angles, stagnation pressure and temperature profiles, and the outlet static pressure, are then prescribed to match the experimental inflow conditions shown in Tab. 2.

Some uncertainty exists with respect to the inflow turbulence specification, since information on the incoming turbulent length scales is not available from the experiment. For the RANS cases an inflow turbulent length scale of 4 mm was chosen, since this agreed well with previous RANS studies [8, 15]. This choice is rather arbitrary, however it is also close to the value of 5 mm chosen by Gourdin [17] for a similar compressor case. With the measured inflow turbulence intensities being quite low, no inflow perturbations are currently applied in the ZDES cases.

NUMERICAL METHOD

To ensure findings can be transferred to an industrial context this investigation uses an industrial RANS CFD code that has been extended to handle LES. The code is the Rolls-Royce CFD code *Hydra* [18], which is an unstructured, mixed element, compressible, density-based Navier-Stokes solver. The unstructured mixed-element approach allows for the computation of complex geometries. However there is a penalty in computation cost compared to a block-structured solver, and unstructured spatial discretisation schemes are generally limited to second order accuracy.

TABLE 2: INLET FLOW CONDITIONS, INCLUDING END-WALL BOUNDARY LAYER PARAMETERS.

| Parameter | Value |
|---|-------------------|
| Reynolds number (Chord based), Re_c | 2.3×10^5 |
| Boundary layer thickness, δ (mm) | 5.23 |
| Displacement thickness, δ^* (mm) | 0.507 |
| Momentum thickness, θ | 1.75 |
| Shape factor, H | 1.35 |
| Flow inlet angle, α_1 ($^\circ$) | 41.0 |
| Incidence angle, i ($^\circ$) | 0.0 |
| Free-stream turbulence intensity (% RMS) | 1.5 |

The main features of the *Hydra* code are summarised below, and modifications made for use as a Hybrid RANS/LES type solver are presented.

Governing Equations

The *Hydra* code solves for the spatially filtered, Favre-averaged, unsteady, compressible Navier-Stokes equations. For the conservative variables these can be expressed as

$$\frac{\partial}{\partial t} \int_{\partial\Gamma} F(Q).n \, dS + \int_{\partial\Gamma} F(Q).n \, dS + \int G(Q).n \, dS = 0 \quad (1)$$

where

$$Q = \begin{bmatrix} \bar{\rho} \\ \bar{\rho}\tilde{u} \\ \bar{\rho}\tilde{v} \\ \bar{\rho}\tilde{w} \\ \tilde{E} \end{bmatrix}, \quad F(Q).n = \begin{bmatrix} \bar{\rho}\tilde{U}_n \\ \bar{\rho}\tilde{U}_n\tilde{u} + n_x\bar{\rho} \\ \bar{\rho}\tilde{U}_n\tilde{v} + n_y\bar{\rho} \\ \bar{\rho}\tilde{U}_n\tilde{w} + n_z\bar{\rho} \\ \tilde{U}_n(\tilde{E} + \bar{\rho}) \end{bmatrix} \quad (2)$$

$$\tilde{U}_n = \tilde{u}n_x + \tilde{v}n_y + \tilde{w}n_z$$

and $G(Q)$ contains viscous and conduction flux terms. In an LES context the notation $\bar{\cdot}$ is for unweighted-filtered variables and $\tilde{\cdot}$ is for density-weighted filtered variables.

Spatial Discretisation

A finite volume discretisation is used, with median-dual control volumes created that surround each node of the mesh. The fluxes through each median-dual control volume face are accumulated to each node by looping over all the edges connecting

the nodes. The inviscid flux $F(Q)$ is computed using the second-order accurate scheme of Moinier [19]. This is based on the flux differencing ideas of Roe [20], which is essentially a central differencing scheme with some element of upwinding for smoothing. For the edge connecting nodes i and j , the inviscid flux is computed as:

$$F_{ij} = \frac{1}{2} [F(Q_i) + F(Q_j)] - \text{smoothing} \quad (3)$$

with the smoothing term given by

$$\text{smoothing} = \frac{1}{2} |A_{ij}| \epsilon (L_j^{lp}(Q) - L_i^{lp}(Q)), \quad (4)$$

where L^{lp} is the pseudo-Laplacian, ϵ is a user-defined smoothing constant, and

$$|A_{ij}| = \partial F / \partial Q. \quad (5)$$

Modifications for LES

It is important for the smoothing term to be minimised in LES regions, to prevent excessive unphysical dissipation of the resolved eddies. This is especially so at low Mach numbers such as those found in the current case. Various approaches have been used by LES practitioners to reduce the smoothing in *Hydra*. It is possible to tune the smoothing constant ϵ in Eqn. 4 to match the flow physics [21], however the value of ϵ isn't designed to act as a global constant and must often be tuned locally. Trial and error can also be used to find the minimum stable value of ϵ [22]. Alternatively, a wiggle detector can be used to adapt the amount of smoothing based on the local level of dispersion [23]. However, the wiggle detectors previously implemented in *Hydra* still require some degree of tuning.

To avoid the need for tuning, Watson [24] instead implemented a Kinetic Energy Preserving (KEP) scheme in *Hydra*. This is based on the work of Jameson [25], and is implemented by simply changing the order of averaging of the flux terms. Instead of multiplying the primitive variables at each node and then averaging them as is done in the original Roe scheme given in Eqn. 1:

$$F_{ij} = \left[\frac{1}{2} \rho_i u_i \phi_i + \frac{1}{2} \rho_j u_j \phi_j \right] - \text{smoothing} \quad (6)$$

in the KEP scheme the primitive variables are instead averaged at each node first, and then multiplied:

$$F_{ij} = \left[\frac{1}{2} (\rho_i + \rho_j) \times \frac{1}{2} (u_i + u_j) \times \frac{1}{2} (\phi_i + \phi_j) \right] - \text{smoothing} \quad (7)$$

At low Mach numbers the conservation of kinetic energy leads to a stability increase that means no artificial dissipation terms are required. Tucker [7] also found that such a scheme is considerably less sensitive to grid quality. However, this is at the expense of some dispersive errors which occur due to the lack of smoothing.

Turbulence Treatments

The different turbulence treatments investigated are summarised in Tab. 3. Three steady RANS approaches were tested; the 1-equation Spalart-Allmaras (SA) model [26] and the 2-equation SST [27] model, both common in industry, were used with *Hydra*. Additionally a Quadratic Pressure-Strain Reynolds Stress Model (RSM) [28] was used with the Ansys *Fluent* commercial CFD solver.

In an attempt to improve the capability of the RANS models for predicting the complex flow physics near the endwall, corrections for streamline curvature/rotation (SARC), turbulence anisotropy (SA-QCR) and non-equilibrium of turbulence (SALSA) are applied to the SA model in *Hydra*. References for these are provided in Tab. 3.

TABLE 3: TURBULENCE TREATMENTS USED.

| Model | Correction(s) used | Abbr. |
|---------------|--|----------|
| SA [26] | Rotation correction [29] | SA |
| | Rotation/curvature correction [30] | SARC |
| | Strain Adaptive formulation of SA model [31] | SALSA |
| | Quadratic Constitutive Relation [32] | SA-QCR |
| SST [27] | Menter production limiter [27] | SST |
| | Kato-Launder production term [33] | |
| RSM [28] | None | RSM |
| SA based ZDES | Same as “SA” configuration | ZDES-SA |
| | Same as “SST” configuration | ZDES-SST |

The hybrid RANS/LES method chosen here is a Zonal Detached Eddy Simulation (ZDES) type approach, similar to that suggested by Deck [34]. The DES methodology [35] involves

using the same RANS model in both RANS and LES regions, which fits in with the strategy of modifying a mature RANS solver for LES. Instead of allowing the model to decide when to transition to LES, as in the case in standard DES type approaches, here the RANS-LES interface is set by the user. This reduces mesh sensitivity and prevents problems such as Grid Induced Separation which the original DES formulation can suffer from [34]. For the SA based ZDES the wall distance function d in the SA model is replaced with a modified distance function:

$$\tilde{d} = \begin{cases} d & \text{if } d < d^{int} \\ C_{DES}^{SA} \Delta_{vol} & \text{otherwise} \end{cases} \quad (8)$$

where $C_{DES}^{SA} = 0.65$. The SST based DES [36] is zonised in a similar manner, with the destruction of turbulent kinetic energy (k) term in the SST model’s k equation multiplied by a function F_{DES} , given by:

$$F_{DES} = \begin{cases} 1 & \text{if } d < d^{int} \\ \frac{L_t}{C_{DES}^{SST} \Delta_{vol}} & \text{otherwise} \end{cases} \quad (9)$$

where L_t represents the $k - \omega$ turbulent length-scale given by $L_t = \sqrt{k}/\omega$. In the LES mode usually only the $k - \varepsilon$ branch of the SST model is important. However, as recommended by Travin et al. [36], Menter’s blending function (F_1) is used to blend the $k - \varepsilon$ and $k - \omega$ C_{DES} constants:

$$C_{DES}^{SST} = (1 - F_1) C_{DES}^{k-\varepsilon} + F_1 C_{DES}^{k-\omega} \quad (10)$$

where $C_{DES}^{k-\varepsilon} = 0.61$ and $C_{DES}^{k-\omega} = 0.78$.

The distance d^{int} is set to $y^+ \approx 60$ as advocated by Deck [34] amongst others. This gives a Wall Modelled LES (WMLES) type approach, where the RANS layer covers only a small part of the boundary layer. Outside of this we have LES type behaviour, with the computational mesh providing an implicit filter for the large eddies.

To reduce the predicted turbulent viscosity on less than ideal (i.e. anisotropic grids) the filter width is changed from the standard DES maximum cell edge length filter $\Delta_{max} = \max(\Delta x, \Delta y, \Delta z)$ to the cubed root of volume $\Delta_{vol} = \sqrt[3]{\Delta x \Delta y \Delta z}$ filter. Finally, as recommended by Breuer et al. [37] the SA model constants are altered in the LES zone

$$f_{v1} = 1, \quad f_{v2} = 0, \quad f_w = 1 \quad (11)$$

This prevents the near-wall damping functions of the SA model interpreting the low-eddy-viscosity levels typical of resolved LES regions as closeness to the wall.

Simulation Time and Numerical Cost

Temporal discretisation is performed with a standard five-stage Runge-Kutta algorithm. The CFL condition limits the time-steps to a small value of 3.2×10^{-8} s. This is due to the very small cells in the endwall-blade surface corners, which is a result of the $y^+ \leq 1$ condition in two directions here. The time-step corresponds to a maximum acoustic CFL of 10 and a maximum convective CFL of 0.8.

Each convective pass consisted of approximately 440000 time-steps. The computations were initialised from the previous steady SA or SST RANS solutions, and were run for one convective pass to flush through the initial transients. The averaging of flow variables was then performed for a further three convective passes. Thus each ZDES computation consisted of approximately 1.76×10^6 time-steps.

The ZDES cases were run on 128 cores on the *Darwin* CPU cluster at the University of Cambridge, with ParMeTis [38] used for domain decomposition. *Hydra* has been found to scale well to over 2000 cores using MPI. The *Darwin* cluster was upgraded in 2012, and now contains 9600 2.60GHz Intel Sandy Bridge cores (600 nodes, 64GB of RAM per node, connected by Mellanox FDR Infiniband). The cost amounted to approximately 41k core hours per ZDES computation, compared to approximately 400 core hours per RANS computation. The small cells in the endwall-blade surface corner mean that the ZDES computations are quite expensive, even with the use of RANS layers to reduce mesh size. The use of an implicit or hybrid explicit-implicit time-stepping scheme could potentially reduce cost here.

DISCUSSION OF RESULTS

RANS Results

Figure 2 shows the measured and computed loss coefficient, Y_p , at the plane shown in Fig. 1. The loss due to the endwall boundary layer and blade wake are visible in both RANS predictions, and the magnitude and extent of these regions are quite similar to the experiment. However, as expected, the SA model cannot correctly predict the complex endwall flow. Hence, the extent of corner separation is over-predicted, and the lift-off of the loss core (darkest red region in Fig. 2b) isn't predicted. The SST model showed similar behaviour here. Figure 2c shows that the more elaborate RSM RANS does better, however the loss distribution still isn't in complete agreement with the measured data.

Gbladebo [1] introduces the use of “relative displacement thickness”, $[\delta^*(z) - \delta_{mid}^*]/c$, to quantify the thickness of the 3D separated region over the suction surface. $\delta^*(z)$ is the local displacement thickness and δ_{mid}^* is the displacement thickness at the blade mid-span. The “relative displacement thickness” across the blade trailing edge is plotted for all the RANS cases in Fig. 3. It is apparent that the pitch-wise and span-wise extents of the corner separation are significantly over-predicted by the SA and SST

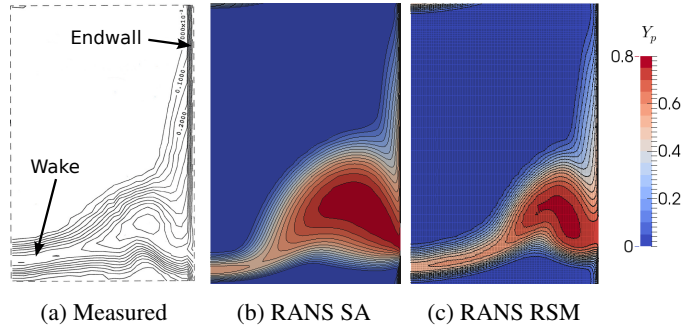


FIGURE 2: LOSS COEFFICIENT CONTOURS 50% DOWNSTREAM OF TRAILING EDGE, FOR RANS CASES.

models. Figure 4a suggests that this leads to under-turning of the flow near the endwall. In a similar manner, Fig. 3 shows that the RSM more accurately predicts the span-wise extent of the corner separation, however the pitch-wise extent is still over-predicted, therefore the flow is still under-turned near the endwall.

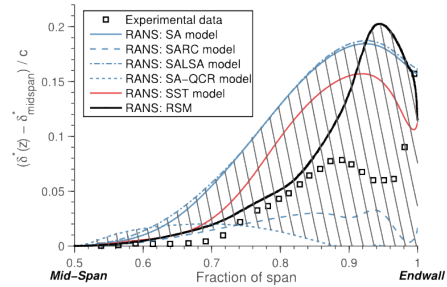


FIGURE 3: RELATIVE DISPLACEMENT THICKNESS ACROSS TRAILING EDGE FOR RANS CASES.

Despite the uncertainty in the predicted extent of the corner separation and exit flow angles, the baseline SA and SST models still provide fairly close agreement with the mass averaged loss predictions at the outflow plane, seen in Fig. 4b. Also, the RSM agrees very well here.

Fig. 5 shows the static pressure coefficient, C_p , distributions on the blade. Near the endwall (Fig. 5b) the SA and SST models both perform quite poorly; the corner separation lifts off too early, and pressure recovery on the latter half of the suction surface is restricted by the overly large corner separation region. Near the mid-span (Fig. 5a) the SA and SST models may be expected to do quite well. However, the the overly large corner separation region contaminates the C_p predictions towards the trailing edge on the suction surface. At both span locations the RSM's C_p predictions are in better agreement with measurements compared to the SA and SST models, however there are still substantial differences.

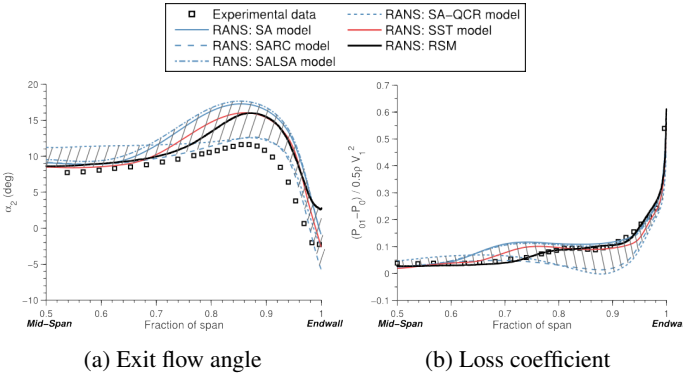


FIGURE 4: SPANWISE DISTRIBUTION OF PITCHWISE MASS AVERAGED PARAMETERS, $0.5c$ DOWNSTREAM FROM TRAILING EDGE. FOR RANS CASES.

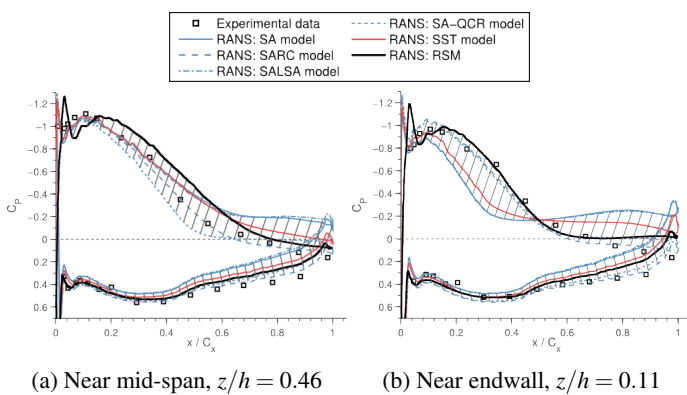


FIGURE 5: C_p DISTRIBUTIONS FOR RANS CASES.

The baseline SA and SST models have been found to struggle in this endwall flow. It is desirable to improve these models without having to resort to more complex or expensive turbulence treatments. However, the hatched areas in Figs. 3-5 show that the RANS corrections tested only serve to add even more uncertainty. The SARC model greatly improves the predicted C_p and exit flow angle distributions, more so than even the complex RSM model. However, it causes the relative displacement thickness to be under-predicted near the endwall, and consequently the total pressure loss here is also significantly underpredicted. Similar results are observed with the SA-QCR model, however this correction worsens the prediction of the exit flow angle near the mid-span. The SALSA model gives similar predictions to the SA model. This is unsurprising since the SALSA correction scales the local turbulent production by altering the SA model's C_{b1} constant ($C_{b1} = 0.1355$ by default) between the range $0.1173 \geq C'_{b1} \geq 0.1515$, depending on the local magnitude of strain rate. Danhua et al. [2] found that $C_{b1} = 0.24$ was required to give a good prediction for this endwall case.

The Importance of Transition

The baseline RANS SA and SST models appear to struggle with this endwall flow, and corrections for turbulence non-equilibrium, turbulence anisotropy, and streamline curvature/rotation did not universally improve predictions. Even the complex RSM model, which many argue are more capable of handling such flows [12], had difficulty here. It is therefore no surprise that there may be other flow physics to consider. For example, the effect of boundary layer transition on the endwall flow. Goodhand and Miller [39] investigate this effect and conclude that any process that thickens the early suction surface boundary layer, for example premature boundary layer transition, may also increase the size of the three-dimensional corner separation.

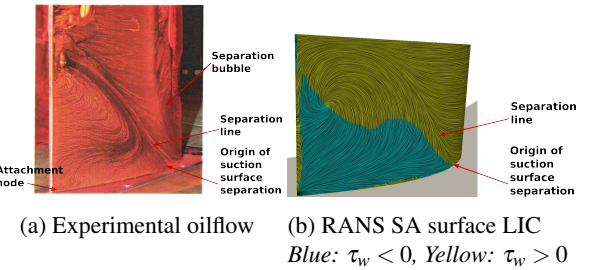


FIGURE 6: SUCTION SURFACE FLOW VISUALISATION FOR EXPERIMENT AND RANS SA CASE.

Figure 6 compares a Line Integral Convolution (LIC) [40] surface flow visualisation from the SA case to the experimental oilflow on the blade's suction surface. It is evident from this that the SA model, like the SST model, doesn't capture the laminar separation bubble and subsequent turbulent reattachment that occur on the suction surface. To investigate whether this affects the corner separation, the SA model case is run with a transition model added.

The transition model, proposed by Kozulovic [41], consists of two modes; natural/bypass mode and separation-induced mode. For both modes, the transition onset and transition development are modelled. The model operates by multiplying the turbulence production and destruction terms in the SA model by the intermittencies γ_P and γ_D . In this case, the separation-induced mode is active on the suction surface of the blade. The mode is modelled by an increasing intermittency (γ_P) in the separation bubble. This region, located between the separation onset and the reattachment point, is characterised by a negative wall shear stress (τ_w). The intermittency γ_P is allowed to take values greater than 1 in the rear part of the separation bubble, which is meant to enable the prediction of more realistic bubble lengths and velocity profiles in the reattached regions [41]. Following the reat-

tachment point the intermittency is decreased to a turbulent value of $\gamma_P = 1$.

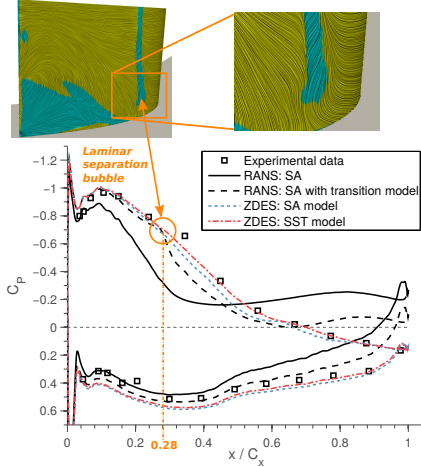


FIGURE 7: C_p DISTRIBUTION NEAR ENDWALL ($z/h = 0.11$) AND SUCTION SURFACE LIC FOR SA WITH TRANSITION MODEL CASE, AND C_p DISTRIBUTION NEAR ENDWALL FOR ZDES CASES.

The effect of adding a transition model on the C_p distribution near the endwall is shown in Fig. 7. The surface flow visualisation and region of negative axial velocity (blue) elucidate the presence of a laminar separation bubble, which is also hinted at by the kink in the C_p distribution at approximately 28% chord. The suction surface boundary layer transition is delayed, and as expected Fig. 8 shows the extent of the corner separation is reduced, leading to a better exit flow angle prediction as seen in Fig. 9a. However, even with a transition model added the extent of the corner separation is still over-predicted. This could possibly be partly due to the predicted transition location being slightly too far upstream, although it is difficult to confirm this from Fig. 7 due to relatively low resolution of experimental data in this region.

With the above analysis in mind it is useful to note that a laminar separation bubble was also observed on the suction surface in the SARC and SA-QRC solutions, and this may help explain why much smaller corner separation regions are seen in these solutions. The SARC model reduces the turbulent viscosity over the suction surface near the leading edge, due to the highly convex streamline curvature here.

Hybrid RANS/LES Results

Addition of a transition model has been found to improve results, however there are still clear deficiencies. There is uncertainty in the predicted transition location, and as other practition-

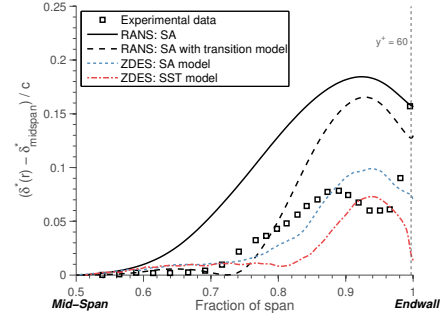


FIGURE 8: RELATIVE DISPLACEMENT THICKNESS ACROSS TRAILING EDGE FOR SA MODEL WITH TRANSITION AND ZDES CASES.

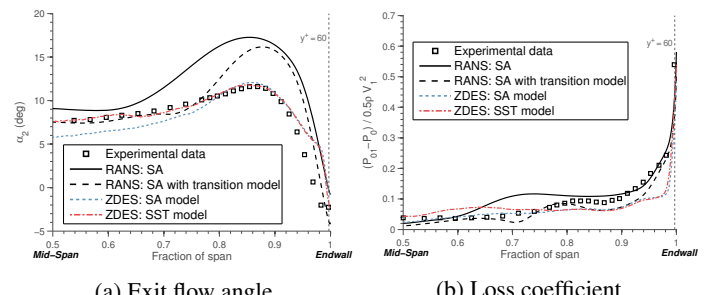


FIGURE 9: SPANWISE DISTRIBUTION OF PITCHWISE MASS AVERAGED PARAMETERS, 50% CHORD DOWNSTREAM FROM TRAILING EDGE. FOR SA MODEL WITH TRANSITION AND ZDES CASES.

ers have found [2, 3, 6], the RANS models struggle to correctly predict the complex turbulence behaviour near the endwall. As an alternative, the ZDES methods aim to resolve much of the complex turbulence that the RANS methods seemed to struggle with. Figure 10 demonstrates this; the steady RANS computation (Fig. 10a) captures some of the key vortical flow structures expected in an endwall flow, for example the suction side leg of the horseshoe vortex system and the suction and pressure side leading edge corner vortices. In the instantaneous ZDES-SST flow field (Fig. 10b) these vortex structures are also captured, in addition to a large amount of turbulent content. The time-averaged ZDES-SST field (Fig. 10c) allows the vortex structures to be seen more clearly. The horseshoe vortex system and leading edge corner vortices are visible. Also, the greater over-turning of the endwall boundary layer means the pressure leg of the horseshoe vortex interacts with the corner vortex to produce the passage and wall vortices.

To further elucidate the differences between the RANS and ZDES flow-fields, stream-tracers for both are presented in Fig. 11. It is apparent that the flow-fields in both cases are topo-

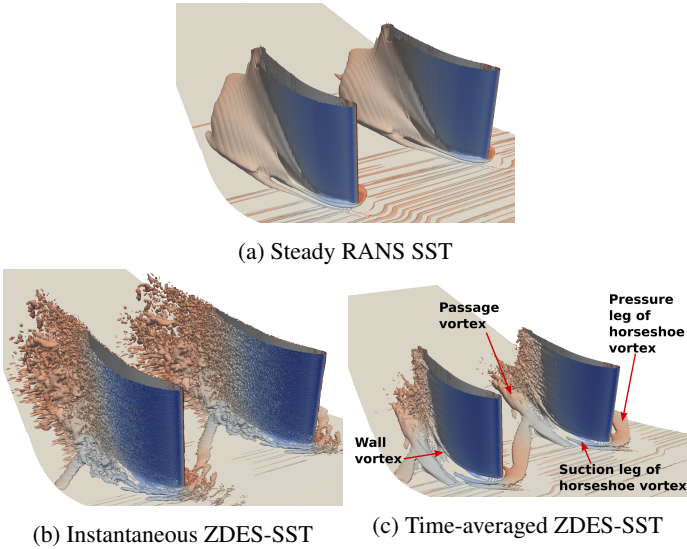


FIGURE 10: ISO-SURFACES OF Q-CRITERION ($Q > 0$), COLOURED BY STATIC PRESSURE, FOR SST BASED RANS AND ZDES CASES.

logically quite different. The ZDES solution shows the vortex system described above, which is similar to that observed by Wang et al. [42] in a turbine endwall flow, and is in agreement with the Gbadebo experiment [1]. Whereas in the RANS solution the corner separation has “opened” and the flow structure is similar to that observed by Wang et al. [9] in a different endwall flow, with a precursor and backbone vortex present.

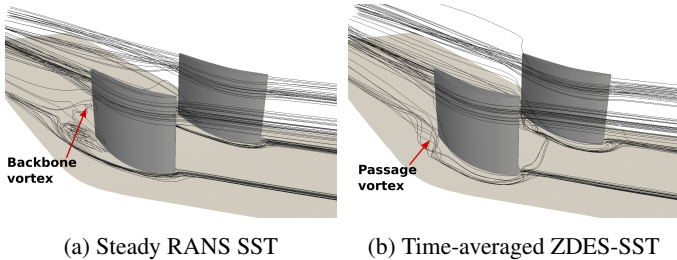


FIGURE 11: STREAM-TRACERS FOR SST BASED RANS AND ZDES.

In addition to the ZDES solutions flow topologies being in closer agreement with the experiment, the extent of the corner separation region is generally in better agreement as seen in Fig. 8. It follows that the C_p (Fig. 7) and exit flow angle (Fig. 9a) distributions for the ZDES-SA and ZDES-SST models are mostly in agreement with the measured data. Interestingly, such agreement is obtained despite the fact that, as shown

in Fig. 7, the ZDES computations don’t resolve the suction surface laminar separation bubble. This is surprising since previous RANS results suggested that correctly capturing the transition process on the suction surface is perhaps important. It is encouraging as it suggests that, at least in the case of a WMLES type hybrid RANS/LES where only a small part of the boundary layer is modelled with RANS, the inclusion of a transition model in the RANS layer isn’t that important. However, more work is required to investigate this area.

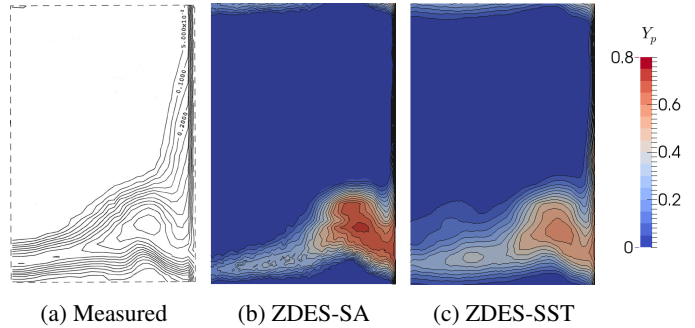
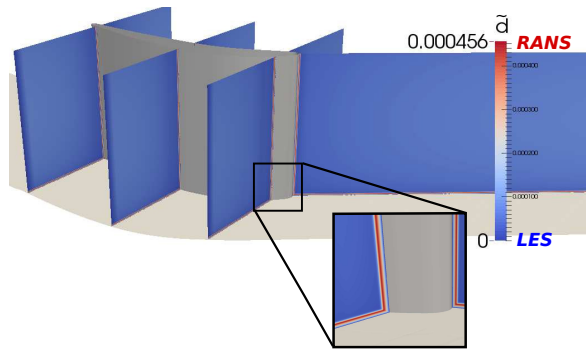


FIGURE 12: LOSS COEFFICIENT CONTOURS 50% DOWNSTREAM OF TRAILING EDGE, FOR ZDES CASES.

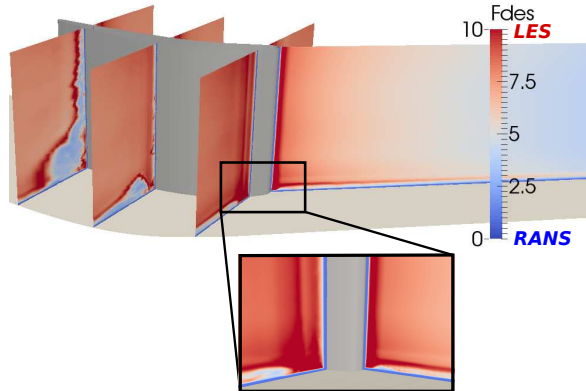
As seen in Fig. 9b the loss predictions are the one area where the ZDES results are slightly disappointing. In both ZDES cases the loss is under-predicted in the endwall region. Examining the loss distributions in Figure 12 it is noticed that the size of the corner separation region is slightly under-predicted, but perhaps more significantly the magnitude of loss in this region is underpredicted, especially close to the endwall. It is thought that this is partly due to a delay in eddy generation here; as discussed by Deck [34] the advection of upstream RANS eddy viscosity can delay the formation of instabilities in mixing layers. The turbulent viscosity is aggressively reduced at $y^+ \approx 60$, but the turbulent fluctuations aren’t immediately formed so we could have a deficit in turbulent content, leading to insufficient loss in the endwall loss core. This hypothesis is supported by the fact that the loss deficit was worse when the step changes in Eqns. 8 and 9 were smoothed with a *tanh* function, which led to a larger “grey area” between the RANS and LES regions.

Overall, both the ZDES solutions agree quite well, however there are a few small differences. For example, the flow is overturned near the mid-span in the ZDES-SA solution (see Fig. 9a), and the high loss region appears more diffused in the ZDES-SST case (Fig. 12c) compared to the ZDES-SA case (Fig. 12b). Since the RANS layers are thin in both cases, it is likely that these differences are at least partly due to differences in the behaviour of the underlying RANS models in the LES regions.

Travin et al. [36] tested the SST based DES model in pure



(a) ZDES-SA: Distribution of effective wall distance, \tilde{d}



(b) ZDES-SST: Distribution of F_{DES} constant

FIGURE 13: ZONALISATION STRATEGIES IN SA AND SST BASED ZDES.

LES mode on a decaying homogeneous isotropic turbulence case, and the resulting Sub-Grid Scale (SGS) model is found to give comparable turbulence spectra to the SA based DES. Also, Figure 13 shows that the SA and SST based ZDES have similar behaviour in the attached boundary layers upstream of the blade; here we have RANS close to the wall ($\tilde{d} = d$ or $F_{DES} = 1$) and LES behaviour away from the walls.

However, once the flow separates clear differences are seen in the LES regions of both ZDES models. In the LES region of the ZDES-SA model $\tilde{d} = C_{DES}\Delta_{vol}$ and so, as seen in Fig. 13a, on a relatively uniform grid the SGS model has fairly uniform behaviour. In contrast, for the ZDES-SST model we have $F_{DES} = L_t/(C_{DES}\Delta_{vol})$ so unlike \tilde{d} the F_{DES} function is dependent on the flow (through $L_t = \sqrt{k}/\omega$) as well as the local grid spacing. Figure 13b shows that this causes the factor F_{DES} to vary greatly across the separated region. In the separated region $F_{DES} \rightarrow 1$ and RANS behaviour is approached. This behaviour seems to go against the philosophy of a zonal hybrid RANS/LES method such as ZDES, where we desire a clear demarcation between RANS and LES zones.

Challenges for RANS

Significant uncertainty has been demonstrated in the RANS predictions, particularly in the endwall flow region. The complex corner separation structure is strongly coupled to the turbulence behaviour. In this section the characteristics of the turbulence near the endwall in the ZDES-SST solution are examined in order to highlight some of the challenges faced by the RANS models.

Under the Boussinesq eddy viscosity assumption, the Reynolds stress is aligned with shear strain. Wang et al. [9] define the misalignment angle between the two as:

$$\alpha_{MA} = \left| \arctan \left(\frac{\partial U}{\partial z} / \frac{\partial V}{\partial z} \right) - \arctan \left(\overline{u'w'}/\overline{v'w'} \right) \right| \quad (12)$$

Figure 14a shows α_{MA} through the blade passage. It appears there is substantial misalignment between the shear strain and Reynolds stress upstream of the corner separation, and this is transported into the corner separation region. This implies the eddy viscosity assumption isn't valid even before the corner separation lift-off. It may be one reason why the linear eddy viscosity RANS models, such as the SA and SST models, struggle here.

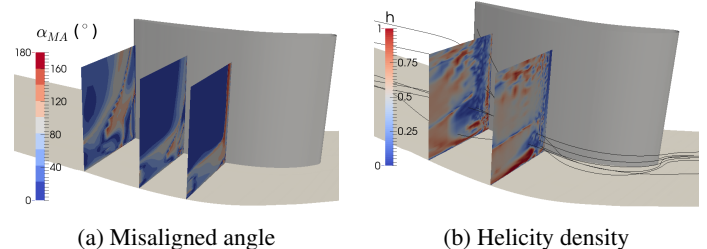


FIGURE 14: MISALIGNMENT ANGLE AND HELICITY DENSITY IN BLADE PASSAGE.

Wang et al. use the velocity helicity density, given by $h = |\boldsymbol{\omega} \cdot \mathbf{u}| / |\boldsymbol{\omega}| |\mathbf{u}|$, to imply the presence of turbulent kinetic energy backscatter in a compressor endwall flow. Liu et al. [43] report that significant backscatter is present when $h > 0.6$. Figure 14b shows that there are high helicity spots throughout the blade passage, with an especially high helicity density close to the passage vortex. This implies the presence of energy backscatter in these regions, which the conventional RANS turbulence models would be unable to predict.

To characterise the Reynolds stress anisotropy in the corner separation region, Lumley triangles [44] are displayed in Fig. 15. Figure 15a shows that at 35% chord the shape of the turbulence

varies substantially across the blade span. In the corner separation region, near the endwall (low z/h), the turbulence is largely two-component axi-symmetric. Very close to the endwall, the stress tensor is disk-like ($\eta = -\xi$) suggesting there is some vortex stretching [45]. Moving away from the endwall the stress tensor becomes more rod-like ($\eta = \xi$), and at the mid-span the turbulence is largely one-component ($\eta = \xi = 1/3$). There is evidently a high degree of turbulence anisotropy here, which will be difficult for the SA and SST models to correctly predict.

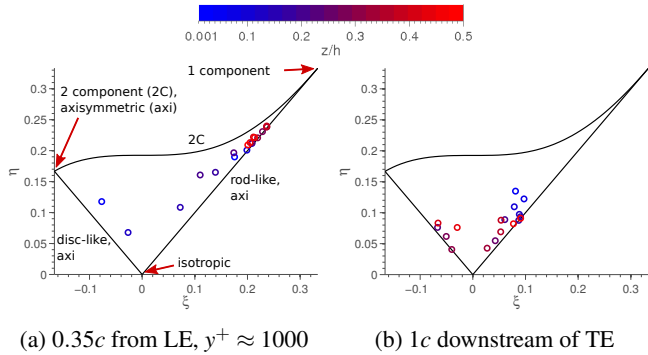


FIGURE 15: LUMLEY TRIANGLES ON $\xi - \eta$ PLANE.

In contrast, 1c downstream of the trailing edge (Fig. 15b) the turbulence can be seen to be returning to isotropy ($\xi = \eta = 0$). This may be less challenging for the RANS models, however there is still substantial unsteadiness and stress-strain misalignment here.

USING LES METHODS IN THE DESIGN PROCESS

Compared to a wall-resolved LES the computational cost of hybrid RANS/LES methods is significantly reduced by modelling the near-wall region with RANS layers. This makes such methods more suitable for application in the turbo-machinery design process. However, this case has highlighted a key challenge; the generation of suitable computational meshes. It seems reasonable to expect the formation of turbulent instabilities to be accelerated if the mesh is finer, so perhaps the loss deficit observed near the endwall is exacerbated by insufficient mesh resolution here. The uncertainty here highlights the need for measures to determine the suitability of the mesh, since hybrid RANS/LES methods are still too expensive for mesh sensitivity studies to be practical in an industrial setting. Additionally, to minimise the number of expensive LES type computations required, tools are needed to guide the generation of the LES mesh in the first place. In the following sections both of these topics are discussed in the context of the endwall flow case.

Meshing from a Precursor RANS solution

Various recommendations exist for grid spacings required in the inner boundary layer for wall-resolved LES [46] and Hybrid RANS-LES [16] computations, and for the outer boundary layer Chapman [47] suggests that around 2500 grid points are required in an averaged volume $\tilde{\delta}^3$ where $\tilde{\delta} = 0.6\delta$. However, LES grid resolution requirements outside of these regions are more difficult to determine, and user experience and/or a priori information of the expected flow-field is often used.

An alternative meshing approach is to use a precursor RANS solution. The idea here is generally to estimate local turbulent length scales using energy budgets, and base the local grid spacing on these length scales, with the aim being to ensure approximately 90% of the turbulent kinetic energy is resolved. The standard inner and outer boundary layer meshing recommendations should still be followed. Piomelli [48] suggests basing the local grid spacing on some fraction of the integral length scale. For the sake of demonstration a fraction of one-tenth gives the required local grid spacing as:

$$\Delta_{int} = \frac{1}{10} \frac{\sqrt{k}}{\omega} \quad (13)$$

Another approach, suggested by Addad et al. [49], is to base the grid spacing on the Taylor microscale L_λ . The reasoning here is that SGS models based on the Boussinesq theory require the implicit cut-off filter width to be in the inertial region of the energy spectrum. The Taylor microscale can be estimated from the RANS SST kinetic energy budget to give the required grid spacing as:

$$\Delta_\lambda = \sqrt{15 \frac{v}{\omega}} \quad (14)$$

The required grid spacings from Equations 13 and 14 are plotted in Figure 16. It is apparent that both resolution criteria give fairly similar spacing requirements, with a coarser mesh being allowed in the corner separation region where larger turbulent length scales are predicted.

One potential problem with the above approaches is that they don't take into account the varying extent of the inertial subrange. A final method, suggested by Tyacke et al. [50], does this by using a modelled energy spectrum proposed by Gamard et al. [51] to estimate the grid spacing required to resolve exactly 90% of the turbulent kinetic energy. Examining the ratio of the integral length scale to the kolmogorov microscale (both obtained with energy budgets from a RANS SST solution), shown in Figure 17a, demonstrates the need to take the length of the inertial sub-range into account. It is found to vary by many orders of magnitude, especially in the separated flow region near the endwall corner.

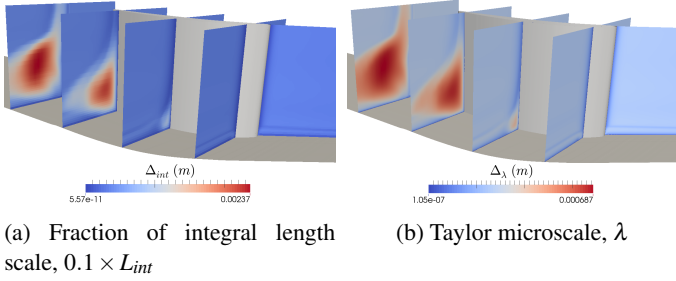


FIGURE 16: LES RESOLUTION REQUIREMENTS BASED ON SOME TURBULENT LENGTH SCALES FROM RANS.

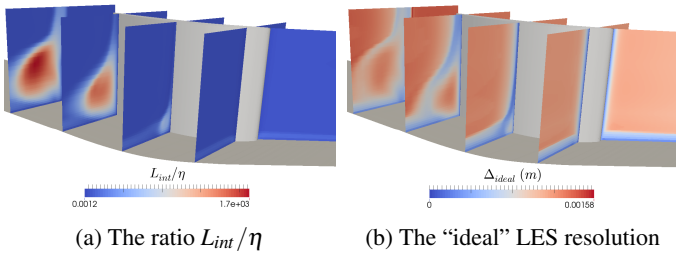


FIGURE 17: THE RATIO OF INTEGRAL LENGTH SCALE TO KOLMOGOROV MICROSCALE AND THE “IDEAL” LENGTH SCALE.

The resulting “ideal” grid resolution requirements obtained from the method of Tyacke et al. [50] are presented in Figure 17b. Interestingly these requirements are quite different to the L_{int} and L_λ based ones shown in Figure 16. The grid spacing required is predicted to be quite coarse in the far field and in the corner separation region, with a fine grid spacing required in the shear layer between the main flow and the separated flow. This makes some sense, since the generation of small turbulent eddies would be expected in this shear layer. Addad et al. [49] didn’t test the Taylor microscale method for separated flows and notes that this is still required, so perhaps this method isn’t suitable for flows such as the endwall one tested here.

All the LES mesh resolution approaches presented suggest there is a large disparity in the mesh scales required in different regions. It is unlikely that such LES meshing requirements can be met with a structured mesh topology without wasting grid points elsewhere in the domain. In fact, in Chapman’s landmark LES meshing requirements paper [47], he notes that some form of nested grid or hanging nodes are required. Examining a summary of recent LES turbo-machinery studies [52] shows that the majority of works use standard structured mesh topologies. Therefore perhaps for LES type cases the use of hanging nodes or unstructured/hybrid meshes warrants further investigation.

Quantifying LES mesh quality

The LES mesh obtained from a precursor RANS solution will only be as “ideal” as the RANS solution was accurate. For example in the current endwall flow the RANS solution over-predicts the size of the corner separation region, which if following the “ideal” grid spacing requirements in Fig. 17b would lead to an overly large region of finer mesh density. Thus in cases where the RANS struggles, such as this one, additional LES mesh quality metrics may be required to check the mesh quality.

Klein [53] and Celik et al. [54] present a number of methods for assessing the quality of an LES computation/mesh. A key challenge is to separate the effect the grid has on the filter size (thus the sub-grid scale model) and the numerical dissipation, therefore empirical methods are usually used to estimate the effect of the numerical scheme, depending on its order of accuracy. The single grid techniques proposed by Celik et al. [54] are examined here, but the numerical dissipation is ignored. This is not completely accurate and ignores the effect of dispersive errors, but since the KEP scheme currently used has extremely low dissipation anyway it should provide a reasonable indication of the mesh quality. The first quality index examined was the sub-grid activity parameter:

$$\tilde{s} = \frac{\bar{v}_t}{\bar{v}_t + v} \quad (15)$$

where \bar{v}_t is the time-averaged turbulent viscosity (from the SGS), and v is the molecular viscosity. However, as Celik et al. [54] note, in most LES applications $v_t \gg v$ therefore $\tilde{s} \approx 1$ and this parameter was not found to be very useful. Instead, the parameter is scaled, as proposed by Celik et al. [54], to give the IQ_v quality index:

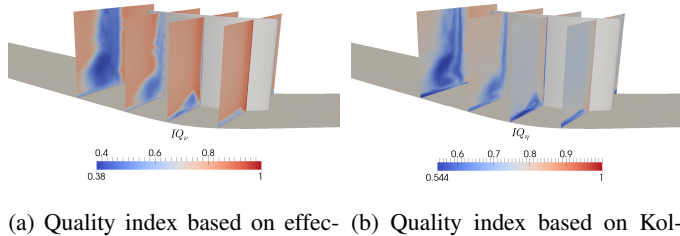
$$IQ_v = \frac{1}{1 + \alpha_v \left(\frac{\bar{v}_t}{v} \right)^n} \quad (16)$$

where $\alpha_v = 0.05$ and $n = 0.53$. These constants are chosen so that IQ_v ranges from 0 to 1, with 0.8 considered a good LES resolution and 0.95 considered DNS. Following a similar design the second quality index is based on the ratio of the local grid spacing Δ to the Kolmogorov microscale L_η :

$$IQ_\eta = \frac{1}{1 + \alpha_\eta \left(\frac{\Delta}{L_\eta} \right)^m} \quad (17)$$

where $\alpha_\eta = 0.05$ and $m = 0.5$. A low value of IQ_v means that the SGS model is more active, which is undesirable since we wish to resolve 90% of the turbulence in all regions. A low value of IQ_η

means that the local grid spacing is significantly larger than the estimated Kolmogorov microscale. Celik et al. [54] states that $\Delta \leq 25\eta_k$ is desirable for LES. However it is unknown whether this is a suitable requirement, and perhaps there is scope to use a different length scale for this index, such as the Δ_{ideal} discussed in the previous section.



(a) Quality index based on effective viscosity (b) Quality index based on Kolmogorov microscale

FIGURE 18: TWO LES QUALITY INDEXES.

These quality indexes were tested on the time-averaged ZDES-SST solution, and the results are shown in Figure 18. This is a hybrid RANS/LES so the results should be ignored in the RANS regions. According to these indexes the mesh used is sufficiently fine upstream of the blade, and in most of the blade passage. However, they suggest the mesh is too coarse in the wake region and in the corner separation region. This could perhaps partly explain the loss deficit observed previously. If the mesh is too coarse, then it will be unable to support sufficient turbulent scales and the generation of turbulence at the RANS-LES interface may also be delayed.

CONCLUSIONS

This paper has demonstrated the potential hybrid RANS/LES methods have for application to turbo-machinery flows, but has also highlighted some of the challenges. The key findings are as follows:

- The steady SA and SST RANS models, and even the much more complex RSM, were found to struggle in this endwall flow. The ZDES-SST solution was used to examine some potential reasons for this. There was significant uncertainty in the C_p and exit flow angle distributions, with the extent of the corner separation over-predicted in both cases. Some RANS corrections were found to offer improvements in some areas, however all of them had significant deficiencies in some areas.
- Transition was found to have a significant effect on the endwall flow. Addition of a transition model to the RANS SA case reduced the premature boundary layer thickening on the

suction surface therefore the extent of the corner separation was not over-predicted as badly.

- The ZDES methods were found to offer encouraging results for this endwall flow. The complex unsteady vortical system near the endwall was well predicted, and despite not capturing the suction surface laminar separation bubble most results were still significantly improved. There were some slight disagreements between the SA and SST based ZDES, and it is thought that this may partly be due the behaviour of the underlying SST model in regions of separated flow. Although the ZDES results were broadly superior to the RANS, the RANS did give better downstream total pressure loss predictions. This is disappointing, however especially in a multi-stage environment the correct predictions of exit flow angles and blockage is thought to be more important, since as Denton [55] notes these will have very dramatic implications on downstream stages if inaccurately predicted. Therefore the ZDES results are considered to be far superior.

- The technique of using a pre-cursor RANS solution to guide LES mesh generation shows promise for this case, however some disagreement was observed between the different strategies proposed in the literature. It may be that different turbulent length scales are more suitable for application in different flows, for example endwall flows versus jets, and further investigation is required here. The work also highlighted the potential for LES quality indexes to be used to provide additional confidence in LES solutions, and these may be especially useful when detailed experimental data is not available for validation work.
- As Chapman [47] notes, the meshing requirements for an eddy resolving simulation are not the same as for a RANS simulation. The “ideal” mesh requirements generated for the endwall flow demonstrate the large disparity in mesh scales required in such a flow. It follows that nested grids, hanging nodes or hybrid (unstructured/structured) meshes may be more suitable than standard multi-block structured meshes for coping with the large range in resolved scales.

ACKNOWLEDGMENT

This work was supported by the Engineering and Physical Sciences Research Council (EPSRC) through an industrial CASE award sponsored by Rolls-Royce plc. Rolls-Royce plc are also gratefully acknowledged for allowing the use and modification of their CFD solver *Hydra*.

The computations described in this paper were carried out on the *Darwin* cluster at the University of Cambridge, and thanks go to the university’s HPC service for their support here.

REFERENCES

- [1] Gbadebo, S. A., Cumpsty, N. A., and Hynes, T. P., 2005. “Three-Dimensional Separations in Axial Compressors”. *Journal of Turbomachinery*, **127**(2), Apr., pp. 331–339.
- [2] Danhua, W., Lipeng, L., and Qiushi, L., 2009. “Improvement on S-A Model For predicting corner separation Based On Turbulence Transport Nature”. *45th AIAA/ASME/SAE/ASEE Joint Propulsion Conference & Exhibit*(August), pp. 1–9.
- [3] Marty, J., Aupoix, B., Schwallinger, M., and Sharma, V. C., 2008. “Effet de la modélisation de la turbulence en proche pompage dans un compresseur multi-étages”. In AAAF, 43ème Colloque d’Aérodynamique Appliquée.
- [4] Langston, L. S., 2001. “Secondary Flows in Axial Turbines-A Review”. *Annals of the New York Academy of Sciences*, **934**(1), Jan., pp. 11–26.
- [5] Horlock, J. H., and Denton, J. D., 2005. “A Review of Some Early Design Practice Using Computational Fluid Dynamics and a Current Perspective”. *Journal of Turbomachinery*, **127**(1), Jan., p. 5.
- [6] Dunham, J., 1998. “CFD Validation for Propulsion System Components”. *AGARD Advisory Report 355*.
- [7] Tucker, P. G., 2013. “Trends in turbomachinery turbulence treatments”. *Progress in Aerospace Sciences*, **63**, Nov., pp. 1–32.
- [8] Klostermeier, C., 2008. “Investigation into the capability of large eddy simulation for turbomachinery design”. PhD thesis, University of Cambridge.
- [9] Wang, Z., and Yuan, X., 2013. “Unsteady mechanisms of compressor corner separation over a range of incidences based on hybrid LES/RANS”. *Proc. of ASME Turbo Expo*, pp. 1–11.
- [10] Riéra, W., Castillon, L., Marty, J., and Leboeuf, F., 2013. “Inlet Condition Effects on the Tip Clearance Flow With Zonal Detached Eddy Simulation”. *Journal of Turbomachinery*, **136**(4), Oct.
- [11] Lardeau, S., Leschziner, M., and Zaki, T., 2011. “Large Eddy Simulation of Transitional Separated Flow over a Flat Plate and a Compressor Blade”. *Flow, Turbulence and Combustion*, **88**(1-2), July, pp. 19–44.
- [12] Morsbach, C., Franke, M., and Mare, F., 2012. “Towards the application of Reynolds stress transport models to 3D turbomachinery flows”. In 7th International Symposium on Turbulence, Heat and Mass Transfer.
- [13] Lien, F. S., and Leschziner, M. A., 1995. “Modelling 2D separation from a high lift aerofoil with a non-linear eddy-viscosity model and second-moment closure”. *Aeronautical Journal*, **99**, pp. 125–144.
- [14] Tucker, P. G., 2014. *Unsteady Computational Fluid Dynamics in Aeronautics*, Vol. 104 of *Fluid Mechanics and Its Applications*. Springer Netherlands, Dordrecht.
- [15] Gbadebo, S. A., 2003. “Three-Dimensional Separations in Compressors”. PhD thesis, University of Cambridge.
- [16] Piomelli, U., 1999. “Large-eddy simulation: Achievements and challenges”. *Prog. Aerospace Sciences*, **35**, pp. 335–362.
- [17] Gourdain, N., 2013. “Validation of large-eddy simulation for the prediction of compressible flow in an axial compressor stage”. In Proc. of ASME Turbo Expo, pp. 1–15.
- [18] Crumpton, P., Moinier, P., and Giles, M., 1997. “An unstructured algorithm for high Reynolds number flows on highly stretched grids”. *Tenth international conference on numerical methods for laminar and turbulent flow*, pp. 1–13.
- [19] Moinier, P., 1999. “Algorithm Developments for an Unstructured Viscous Flow Solver”. PhD thesis, University of Oxford.
- [20] Roe, P., 1986. “Characteristic-Based Schemes for the Euler Equations”. *Annual Review of Fluid Mechanics*, **18**(1), Jan., pp. 337–365.
- [21] Eastwood, S. J., Tucker, P. G., Xia, H., and Klostermeier, C., 2009. “Developing large eddy simulation for turbomachinery applications”. *Philosophical transactions. Series A, Mathematical, physical, and engineering sciences*, **367**(1899), July, pp. 2999–3013.
- [22] McMullan, W. A., and Page, G. J., 2012. “Towards Large Eddy Simulation of gas turbine compressors”. *Progress in Aerospace Sciences*, **52**, July, pp. 30–47.
- [23] Ciardi, M., 2005. “Large Eddy Simulation for broad-band noise in turbomachinery”. PhD thesis, University of Cambridge.
- [24] Watson, R., 2013. “Large Eddy Simulation of Cutback Trailing Edges for Film Cooling Turbine Blades”. PhD thesis, University of Cambridge.
- [25] Jameson, A., 2007. “Formulation of Kinetic Energy Preserving Conservative Schemes for Gas Dynamics and Direct Numerical Simulation of One-Dimensional Viscous Compressible Flow in a Shock Tube Using Entropy and Kinetic Energy Preserving Schemes”. *Journal of Scientific Computing*, **34**(2), Dec., pp. 188–208.
- [26] Spalart, P. R., and Allmaras, S. R., 1994. “A one-equation turbulence model for aerodynamic flows”. *Recherche Aerospatiale*, **1**, pp. 5–21.
- [27] Menter, F. R., Kuntz, M., and Langtry, R., 2003. “Ten Years of Industrial Experience with the SST Turbulence Model”. *Turbulence Heat and Mass Transfer 4*, **4**, pp. 625–632.
- [28] Speziale, C. G., Sarkar, S., and Gatski, T. B., 2006. “Modelling the pressurestrain correlation of turbulence: an invariant dynamical systems approach”. *Journal of Fluid Mechanics*, **227**, Apr., p. 245.
- [29] Dacles-Mariani, J., Zilliac, G. G., Chow, J. S., and Bradshaw, P., 1995. “Numerical/experimental study of a wingtip vortex in the near field”. *AIAA Journal*, **33**(9), Sept., pp. 1561–1568.

- [30] Spalart, P., and Shur, M., 1997. "On the sensitization of turbulence models to rotation and curvature". *Aerospace Science and Technology*, **1**, pp. 297–302.
- [31] Rung, T., Bunge, U., Schatz, M., and Thiele, F., 2003. "Restatement of the Spalart-Allmaras Eddy-Viscosity Model in Strain-Adaptive Formulation". *AIAA Journal*, **41**(7), July, pp. 1396–1399.
- [32] Spalart, P. R., 2000. "Strategies for turbulence modelling and simulations". In *International Journal of Heat and Fluid Flow*, Vol. 21, pp. 252–263.
- [33] Kato, M., and Launder, B. E., 1993. "The Modelling of Turbulent Flow Around Stationary and Vibrating Square Cylinders". In *9th Symposium on Turbulent Shear Flows*, pp. 10.4.1–10.4.6.
- [34] Deck, S., 2005. "Zonal-Detached-Eddy Simulation of the Flow Around a High-Lift Configuration". *AIAA Journal*, **43**(11), Nov., pp. 2372–2384.
- [35] Spalart, P., Jou, W., Strelets, M., and Allmaras, S., 1997. "Comments of the feasibility of LES for wings, and on a hybrid RANS/LES approach". In *Proceedings of the First AFOSR International Conference on DNS/LES*, C. Liu and Z. Liu, eds., pp. 137–147.
- [36] Travin, A. K., Shur, M. L., Strelets, M. K., and Spalart, P. R., 2000. "Physical and Numerical Upgrades in the Detached-Eddy Simulation of Complex Turbulent Flows". In *Advances in LES of Complex Flows*, R. Friedrich and W. Rodi, eds. Kluwer Academic Publishers, pp. 239–254.
- [37] Breuer, M., Jovicic, N., and Mazaev, K., 2003. "Comparison of DES, RANS and LES for the separated flow around a flat plate at high incidence". *International Journal for Numerical Methods in Fluids*, **41**(4), Feb., pp. 357–388.
- [38] Karypis, G., and Kumar, V., 1998. "A Fast and High Quality Multilevel Scheme for Partitioning Irregular Graphs". *SIAM Journal on Scientific Computing*, **20**(1), Jan., pp. 359–392.
- [39] Goodhand, M. N., and Miller, R. J., 2012. "The Impact of Real Geometries on Three-Dimensional Separations in Compressors". *Journal of Turbomachinery*, **134**(2), p. 021007.
- [40] Cabral, B., and Leedom, L. C., 1993. "Imaging vector fields using line integral convolution". In *Proceedings of the 20th annual conference on Computer graphics and interactive techniques - SIGGRAPH '93*, ACM Press, pp. 263–270.
- [41] Kozulovic, D., and Lapworth, B. L., 2009. "An Approach for Inclusion of a Nonlocal Transition Model in a Parallel Unstructured Computational Fluid Dynamics Code". *Journal of Turbomachinery*, **131**(3), July.
- [42] Wang, H. P., Olson, S. J., Goldstein, R. J., and Eckert, E. R. G., 1997. "Flow Visualization in a Linear Turbine Cascade of High Performance Turbine Blades". *Journal of Turbomachinery*, **119**(1), Jan., p. 1.
- [43] Liu, Y., Lu, L., Fang, L., and Gao, F., 2011. "Modification of SpalartAllmaras model with consideration of turbulence energy backscatter using velocity helicity". *Physics Letters A*, **375**(24), June, pp. 2377–2381.
- [44] Lumley, J. L., and Newman, G. R., 1977. "The return to isotropy of homogeneous turbulence". *Journal of Fluid Mechanics*, **82**(01), Apr., pp. 161–178.
- [45] Simonsen, A. J., and Krogstad, P.-A., 2005. "Turbulent stress invariant analysis: Clarification of existing terminology". *Physics of Fluids*, **17**(8), Aug., p. 088103.
- [46] Piomelli, U., and Chasnow, J. R., 1996. "Large-eddy simulations: theory and applications". In *Transition and turbulence modelling*, D. Henningson, M. Hallbäck, H. Alfredsson, and A. Johansson, eds. Kluwer Academic Publishers, Dordrecht, pp. 269–336.
- [47] Chapman, D. R., 1979. "Computational aerodynamics development and outlook". *AIAA Journal*, **17**, pp. 1293–1313.
- [48] Piomelli, U., 2014. "Large-eddy simulations in 2030 and beyond". *Philosophical transactions. Series A, Mathematical, physical, and engineering sciences*, **372**.
- [49] Addad, Y., Gaitonde, U., Laurence, D., and Rolfo, S., 2008. "Optimal Unstructured Meshing for Large Eddy Simulations". In *Quality and Reliability of Large-Eddy Simulations*. pp. 93–103.
- [50] Tyacke, J., Tucker, P. G., Jefferson-Loveday, R., Rao Vadlamani, N., Watson, R., Naqavi, I., and Yang, X., 2013. "Large Eddy Simulation for Turbines: Methodologies, Cost and Future Outlooks". *Journal of Turbomachinery*, **136**(6), Nov.
- [51] Gamard, S., and George, W. K., 2000. "Reynolds Number Dependence of Energy Spectra in the Overlap Region of Isotropic Turbulence". *Flow, Turbulence and Combustion*, **63**(1-4), Jan., pp. 443–477.
- [52] Gourdain, N., Sicot, F., Duchaine, F., and Gicquel, L., 2014. "Large eddy simulation of flows in industrial compressors : a path from 2015 to 2035". *Philosophical transactions. Series A, Mathematical, physical, and engineering sciences*, **372**(2022).
- [53] Klein, M., 2005. "An Attempt to Assess the Quality of Large Eddy Simulations in the Context of Implicit Filtering". *Flow, Turbulence and Combustion*, **75**(1-4), Dec., pp. 131–147.
- [54] Celik, I. B., Klein, M., and Janicka, J., 2009. "Assessment Measures for Engineering LES Applications". *Journal of Fluids Engineering*, **131**(3).
- [55] Denton, J., and Pullan, G., 2012. "A numerical investigation into the sources of endwall loss in axial flow turbines". In Proc. of ASME Turbo Expo, pp. 1–14.